International Journal of Hydrogen Energy 137 (2025) 925–938

Contents lists available at ScienceDirect

International Journal of Hydrogen Energy

journal homepage: www.elsevier.com/locate/he

Hydrogen-fuelled internal combustion engines: Direct Injection versus Port-Fuel Injection

Fabián Musy, Rafael Ortiz, Inmaculada Ortiz, Alfredo Ortiz *

Chemical & Biomolecular Engineering Department, Universidad de Cantabria, Av. Los Castros 46, 39005, Santander, Spain

ARTICLE INFO

Handling Editor: Ibrahim Dincer

Keywords:
Internal combustion engine
Hydrogen
Direct injection
Port-fuel injection
CFD simulation
Hydrogen combustion

ABSTRACT

The road-transport is one of the major contributors to greenhouse global gas (GHG) emissions, where hydrogen (H_2) combustion engines can play a crucial role in the path towards the sector's decarbonization goal. This study focuses on comparing the performance and emissions of port-fuel injection (PFI) and direct injection (DI), in a spark ignited combustion engine when is fuelled by hydrogen and other noteworthy fuels like methane and coke oven gas (COG). Computational fluid dynamic simulations are performed at optimal spark advance and air-fuel ratio (λ) for engine speeds between 2000 and 5000 rpm. Analysis reveals that brake power increases by 40% for DI, attributed to 30.6% enhanced volumetric efficiency, while the sNOx are reduced by 36% compared to PFI at optimal $\lambda = 1.5$ for hydrogen. Additionally, H_2 results in 71.8% and 67.2% reduction in fuel consumption compared to methane and COG respectively, since the H_2 lower heating value per unit of mass is higher.

1. Introduction

The new wave of hydrogen related studies and technological development has mainly shaken Europe due to the eagerness of achieving the goal of net zero greenhouse gases (GHGs) emissions by 2050. In this sense, transport sector represents the 25% of GHGs in the European Union (EU), and hence the European Green Deal demands a 90% emissions reduction by 2050 [1].

To address the problem of emissions related to road transport, key actors in energy transition such as public authorities and private motor companies are gradually transitioning from conventional technologies as internal combustion engines (ICEs) to electric vehicles and alternative fuels. In this sense, H_2 fuelled internal combustion engines (H_2-ICEs) and fuel cell electric vehicles (FCEV) are suitable options to reduce the environmental impacts arising from conventional vehicles. Moreover, H_2-ICEs may ease the transition towards low carbon mobility in a more economical way thanks to the upgrading of current ICEs without requiring the presence of batteries and fuel cells. However, even though the use of H_2 as fuel achieves zero CO_2 emissions during combustion, it has associated nitrogen oxides (NOx) emissions [1,2].

Regarding the application of H_2 in ICEs, the H_2 molecule exhibits distinct intrinsic physicochemical properties compared with conventional fuels and other alternatives, including CH_4 and coke oven gas (COG), a residual stream arising from coke production and valorised as by-product, which consists predominantly of a H_2–CH_4 blend, as detailed in Table 1 [3–7].

The H_2 molecule is the only one free of carbon atoms, offering a clean combustion in terms of GHG. Additionally, the lower heating value (LHV), which represents the energy released during fuel combustion per unit of mass, is nearly three times higher than conventional fuels, CH_4 and COG, proving the high potential of H_2 as clean energy vector. However, it has the lowest density as a consequence of the lower molecular weight, and hence, power density is penalized in gas phase, being measured per unit of volume. Finally, regarding the higher laminar flame speed (S_L) of H_2, it helps improve the combustion efficiency, throughout the improvement in chemical reactivity [8].

Afterwards, different types of configurations which combine the ignition mechanism and injection strategies are reproduced in H_2-ICEs such as spark ignition (SI) coupled with direct or port-fuel injection (DI or PFI), and compression ignition (CI) [7].

Port-fuel injection with spark ignition (SI-PFI) is the most common strategy, which is based on injecting H_2 into the intake manifold instead of directly into the combustion chamber [9–14]. In H_2 SI-PFI systems the variation on the air-fuel ratio (λ) exerts great influence on engine performance. The relative λ factor, represents the proportion of air per unit of mass of fuel in the mixture and is expressed as the coefficient of the real air-fuel ratio (λ_{real}) obtained in the simulations or bench test and the stoichiometric factor (λ_{St}), as defined in Eq. (1) [9].

* Corresponding author.
E-mail address: ortizal@unican.es (A. Ortiz).

https://doi.org/10.1016/j.ijhydene.2024.07.136
Received 27 February 2024; Received in revised form 24 May 2024; Accepted 9 July 2024
Available online 16 July 2024

Nomenclature

A	Area (cm^2)
BMEP	Brake mean effective pressure (bar)
BSFC	Brake specific fuel consumption (g/kWh)
BTE	Brake thermal efficiency (%)
CAD	Crank angle degrees (°)
CHR	Chemical heat release (J)
dBTDC	Degrees before top dead centre (°)
dATDC	Degrees after top dead centre (°)
dBBDC	Degrees before bottom dead centre (°)
dABDC	Degrees after bottom dead centre (°)
EOI	End of injection (°)
$H_R(T_A)$	Reagent enthalpy (J)
$H_P(T_A)$	Product enthalpy (J)
HP	Horse power (HP)
LHV	Lower heating value (MJ/kg)
MBT	Maximum brake torque (N·m)
N	Engine speed (rpm)
PW	Pulse width (°)
SA	Spark advance (°)
S_L	Laminar flame speed (m/s)
sNOx	Specific nitrogen oxides (g/kWh)
SOI	Start of injection (°)
T	Torque (N·m)
TDC	Top dead centre (°)
V_d	Cylinder volume displacement (L)
v_i	Injection velocity (m/s)
$W_{c,i}$	Work delivered per cycle (J/cycle)
WHT	Wall heat transfer (J)
p	Pressure (bar)
P	Power (kW)
P_{Inj}	Injection Pressure (bar)
ρ_i	Density (kg/m^3)
$\rho_{a.i}$	Air density at atmospheric conditions (g/cm^3)
η_e	Volumetric efficiency (%)
$\dot{m}$	Mass flow (g/s)
$\dot{m}_e$	Air mass inlet flow (g/h)
m_a	Real air mass (g)
$\dot{m}_f$	Mass flow of fuel injected per cycle (g/s)
m_{full}	Total mass of fuel injected per cycle (g)
λ	Relative air-fuel ratio
λ_{St}	Stoichiometric air-fuel ratio
λ_{real}	Real air-fuel ratio
η_R	Number of crank revolutions for each power stroke per cylinder

Abbreviations

CFD	Computational fluid dynamics
CI	Compression ignition
COG	Coke oven gas
CR	Compression ratio
DI	Direct injection
EU	European union
FCEV	Fuel cell electric vehicles
GHGs	Greenhouse gases
H_2-ICE	Hydrogen fuelled internal combustion engine
HPDI	High pressure direct injection
ICE	Internal combustion engine
PFI	Port-fuel injection
rpm	Revolutions per minute
SI	Spark ignition
SI-DI	Spark ignition – direct injection
SI-PFI	Spark ignition – port-fuel injection
WOT	Wide open throttle

$$\lambda = \frac{\lambda_{real}}{\lambda_{St}} \quad (1)$$

Thus, according to Verhelst et al., operating at λ equal to 1.4, a 50% net power output is achieved in comparison with the stoichiometric (1:1) air-fuel proportion ($\lambda = 1$). This enhancement is attributed to the synergistic effects of a turbocharger and an exhaust gas recirculation (EGR) system [15]. Furthermore, in the research conducted by Tang et al. a 65% of power output obtained in the same engine powered by gasoline can be obtained through a more precise optimization of the λ factor [16]. Despite the lower power output compared to gasoline engines, Tang et al. demonstrates that the engine brake thermal efficiency (BTE), defined as the ratio of the mechanical energy extracted from the ICE to the fuel consumed, can be enhanced to 38%, surpassing that of gasoline engines [17].

In addition, in PFI H_2-ICEs fuelled by H_2, the power outputs usually range between 4.8 and 66.7 kW for engines volumes from 0.27 L (motorbikes) to 3.984 L (heavy-duty vehicles), and BTE values in the range 22.7–38% [18].

On the other side, DI configuration is based on injecting H_2 directly into the combustion cylinder while the compression stroke takes place, improving the engine performance by avoiding the displacement of air. This results in a higher volumetric efficiency and thus, in higher power density than PFI systems [19].

Regarding the main differences between the PFI and the DI systems, in the latter, the injector system is positioned in the head, allowing the transport of the fuel directly to the cylinder [8]. Thus, several studies have demonstrated that high pressure direct injection (HPDI) can achieve similar efficiencies to diesel engines. Mathias et al. show that operating under ultra-lean conditions ($\lambda = 3.3$), BTE reaches a 35% in most tests [20]. Mohammadi et al., also achieves a maximum BTE of

Table 1
Properties of fuels at standard conditions [3–7].

Parameter	Unit	Gasoline	Diesel	Hydrogen	Methane	Coke Oven Gas
Chemical Formula		C_4–C_{12}	C_8–C_{25}	H_2	CH_4	COG
Composition (C, H, O, N)	Mass-%	84,16,0,0	86,14,0,0	0,100,0,0	25,75,0,0	24,46,16,14
Lower heating value (LHV)	MJ/kg	43.9	42.5	119.9	45.8	39.9
Density	kg/m^3	730–780	830	0.089	0.72	0.41
Stoichiometric air/fuel ratio	kg/kg	14.7	14.5	34.4	17.2	12.72
Flammability limits	Vol-%	1.0–7.6	0.6–5.5	4.0–76.0	5.3–15.0	4.4–34.0
Laminar flame speed in air	m/s	0.37–0.43	0.37–0.43	1.85	0.38	0.68–0.88
Auto-ignition temperature	K	≈623	≈523	853	813	≈673

35% operating at lean conditions ($\varphi = 0.5$; $\lambda = 2$) [21]. Finally, Oikawa et al. obtained a wide range of BTE results due to the different DI approaches studied achieving a maximum of 45% [22].

Likewise, due to the shorter residence time of the fuel inside the engine, thermal efficiency values between 34 and 45.5% are obtained, using engine volumes ranging from 0.66 (motorbikes) to 7.75 L (heavy-duty vehicles), even increasing power by up to 20 % compared to PFI [17,20–27].

Thus, in pursuit of enhanced engine performance, this configuration has adopted a range of injection strategies, encompassing optimized duration and timing, alongside multi-injection strategies utilizing two or more pulses per cycle [8].

Furthermore, the adoption of direct injection with spark ignition (SI-DI) techniques effectively eradicated combustion anomalies such as knock and backfiring. In these engines, direct H_2 injection promotes a more homogeneous distribution of air-fuel mixture, thereby mitigating the occurrence of backfiring. This approach, coupled with H_2 injection at the beginning of compression stroke, prevents knock phenomena [20,28].

Regarding NOx, DI engines result in a 20% reduction compared to NOx levels observed in diesel engines operating at full load for maximum power output [5,8]. In addition, they exhibit a strong dependence on fuel load, showing that the results of early injection strategies increase NOx emissions, and hence, late injection is preferable at partial and low loads [8].

According to the adaptation of the ICE to be directly powered by H_2, some minor modifications are required, for instance, changes in the hardware side, such as the outplacement of fuel injectors, fuel lines, charcoal filters and fuel rail and the optimization of the injection system paying special attention to the aspects of sealing and lubrication, with the aim of achieve an adequate combustion reaction [27,29–32].

Moreover, the injection strategy has a significant impact on DI performance and NOx formation. In this context, there are two main types of DI systems; low-pressure direct injection (LPDI) and high-pressure direct injection (HPDI). The type of injection has to be incorporated with a well-defined injection strategy, which in turn must be in synergy with ignition timing both in PFI and DI [8]. Thus, multiple DI strategies can be differentiated before and after the spark occurs, while in single DI is divided in late and early injections.

In H_2 combustion, λ ratio variations exert a significant influence on combustion velocity and temperature**.** As reported by Luo et al., λ values surpassing 1.67 yield a maximum combustion temperature below 1600 K [33]. This temperature is insufficient to furnish the activation energy required for complete combustion, leading to a degradation of engine efficiency [34]. Conversely, Eichlseder et al., maintain that combustion temperatures must be held below 1800 K to prevent the formation of harmful NOx emissions. This critical threshold is reached at λ lower than 1.4 [18]. Therefore, the optimum λ must be found ranging between 1.4 and 1.67.

Despite de existence of various works addressing the distinctions between DI and PFI engines, none quantitatively delve into the advancements and outcomes of converting petrol-fuelled ICEs to run on H_2. Under this framework, the primary contributions of the present study are referred to the technological implementation and comparison of the performance between PFI-SI H_2-ICEs and high performance H_2-ICEs approaches, mostly based on DI-SI configurations. Moreover, other fuels such as CH_4 and COG have been assessed in order to validate the engine design in e-fuel applications, comparing them with H_2.

This comparison was conducted through computational fluid dynamic (CFD) simulations of both engines and based on performance and emission parameters such as brake power, torque, brake mean effective pressure (BMEP), brake specific fuel consumption (BSFC), brake thermal efficiency (BTE), volumetric efficiency, chemical heat release (CHR) and specific nitrogen oxides emissions (sNOx).

2. ICE design and CFD simulation

2.1. Geometrical design

An experimental bench of a naturally aspirated Volkswagen Polo 1.4 L SI-PFI internal combustion engine with a compression ratio (CR) 10.5:1 was tested and computationally reproduced in a previous work reported by our research group [29]. In that work, the engine was first adapted to be fuelled by gaseous fuels. Those modifications mainly include a replacement of the plastic inlet manifold by a cast manifold and the substitution of gasoline injectors by H_2 injectors in stainless steel 316L, preventing gas-fuel leakages.

In the is study, the original Volkswagen engine was computationally modified to switch from PFI to DI strategy. Firstly, the new designed geometry was reproduced on Autodesk Inventor as can be seen in Fig. 1, highlighting the new shape of the intake manifold and the location of the direct injector.

The main changes in comparison with the PFI geometry model involved the removal of the gas inlet on the intake manifold, giving geometrical continuity. This modification allows better flow of gas and avoids the creation of turbulences. Subsequently, the location of the direct injector on the head of the engine is defined to avoid the interruption of the valve and piston movement paths. Furthermore, the DI system was intentionally designed to employ identical CR and displacement volume (V_d), ensuring a comparison under consistent conditions.

The injector was designed to spray fuel through 5 nozzles positioned 72° apart and inclined 50° relative to the vertical axis of the geometry. The number and arrangement of the nozzles were optimized to enhance fuel dispersion within the cylinder, minimize injection duration, and to expand the start of injection (SOI) range. Consequently, the injector was positioned slightly off-centre from the cylinder head to accommodate the spark plug as in a real engine. In this case, the spark plug is tilted with regard to the vertical axe.

Therefore, the spark and the H_2 sprayed will intersect close to the central axe of the cylinder, where chemical reaction starts. In addition, the air-fuel mixture working with early injection timing and 5-nozzle configuration is normally concentrated on the centre of the cylinder, generating a stratified and more enriched mixture for a better combustion reaction [35].

Finally, a 6.71 mm diameter was implemented based on the number of nozzles and the nozzle diameter of 0.61 mm, which was selected from well stablished studies on 5-nozzle configurations [36].

In this context, among various configurations, the 5-nozzle spray injector was selected for the superior ability of this configuration to promote a favourable mixture stratification, enhancing thermal efficiencies, without compromising NOx emissions working with λ close to 2, and avoiding complexities of other injection systems, which will be crucial to compare DI and PFI engine configurations [35].

The dedicated design is oriented to spark ignition and HPDI strategy, working under low loads of fuel with air-fuel ratios which ranges from 1.5 to 2 in the case of H_2 simulations. Thus, the low loads with early injection strategy and spark plug ignition in HPDI is the best option to obtain high brake power outputs while preventing high NOx formation, which reaches the theoretical peak at air-fuel ratios of 1.25 [8].

In this case, the early DI also offers an homogeneous mixture which helps to improve thermal efficiency and reduce NOx through a reduction in combustion temperature, even in comparison with PFI. Moreover, the general behaviour related to the existent trade-off between fuel load and NOx formation also applies to PFI systems. For this reason, early DI strategy is selected [8].

Finally, the closing and opening valve profiles in both engine configurations are the same and do not change with the variation in spark advance (SA) and start of injection (SOI) or end of injection (EOI). In this context, the main values about angles and distances are collected in Table 2.

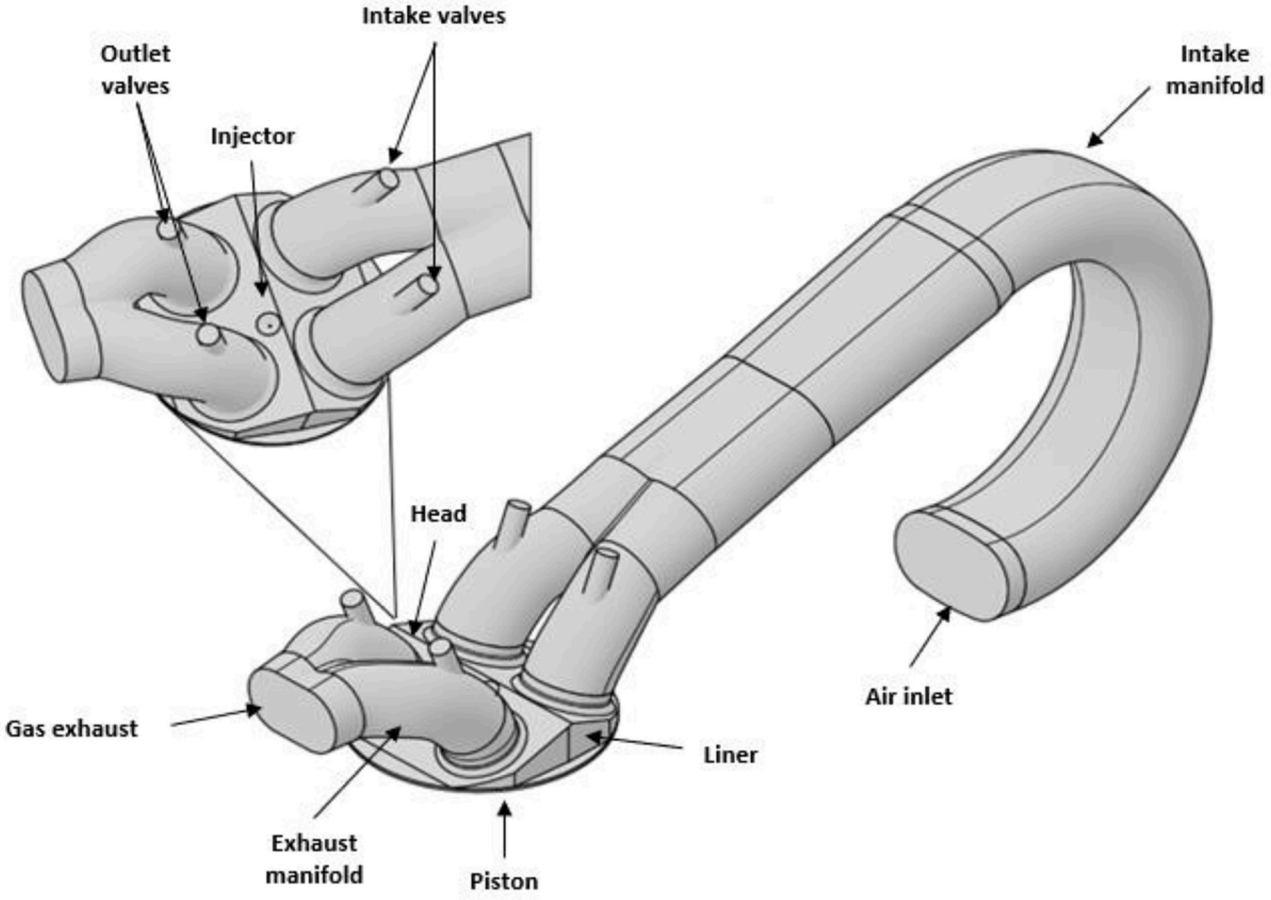

Fig. 1. Geometrical DI engine design.

Table 2
Valve profiles main values.

Intake Valves Profiles		
Opened (IVO, ∘)	Closed (IVC, ∘)	Max. Lift (cm)
18.2	15.2	0.84
Exhaust Valve Profiles		
Opened (EVO, ∘)	Closed (EVC, ∘)	Max. Lift (cm)
19.4	16.4	0.86

Thus, the valve profiles remain unchanged across both configurations to ensure consistent operation comparable to the Volkswagen Polo 1.4L PFI. Therefore, this model has been implemented with minimal geometric changes, without altering the exhaust mixture evacuation times or air intake timings. This approach allows for a focused assessment of the resultant advantages and disadvantages derived solely from changing the injection system and the intake manifold shape. Conversely, the valve profiles are also maintained to get a suitable synergy among the different parts of the engine avoiding physical collisions between valves and piston which have been configured as moving parts.

2.2. CFD Simulation

The designed geometrical model is imported to ANSYS Workbench to be adapted on the computational aided design tool ANSYS SpaceClaim and meshed on ANSYS Meshing to prepare the geometry. Subsequently, simulations were carried out in the computational fluid dynamics (CFD) simulation tool ANSYS Forte.

The combustion chemistry of H_2, CH_4 and COG is first introduced. Consequently, a chemical reaction pathway must be imported. In this regard, identifying a mechanism that accurately represents the combustion of each fuel is critical as all results hinge on combustion modelling. Therefore, the most comprehensive mechanism, GRI-Mech 3.0, is implemented. The GRI-Mech 3.0 effectively models H_2 and CH_4, including all their possible reactions, and COG, defined as a mixture of several gases such as H_2, CH_4, nitrogen (N_2), carbon dioxide (CO_2) and carbon monoxide (CO) demonstrating the model completeness. Thus, this reaction model developed by the University of California, in Berkeley, comprises 325 reactions and 53 species [37].

In this sense, the GRI-Mech 3.0 optimizes the combustion reactions carried out within a temperature range among 1000 and 2500 K and air-fuel ratios from 0.2 to 10. In addition, run simulations over this validation ranges could be also reasonable, as elementary reactions encompasses all the required steps deemed crucial for describing the combustion and flame propagation, including the reduction or formation of NOx [37].

The definition of the reaction mechanism is essential to establish operational parameters, a critical step in achieving optimal performance in H_2-ICE simulations. Accordingly, spark characteristics are defined to determine their crankshaft angle duration (CAD), using Eq. (2). This calculation utilizes the nominal spark angle (720°), spark time (ms), and engine speed (N) (rpm).

$$Duration = N\left(\frac{rev}{min}\right) \cdot \frac{1\ min}{60\ s} \cdot \frac{360\ CAD}{1\ rev} \cdot 1\ ms \cdot \frac{1 \cdot 10^{-3}\ s}{1\ ms} \quad (2)$$

Furthermore, the spark advance, which characterizes the timing of spark ignition, is derived from the values previously gathered in the experimental bench and reported by our research group [18]. Therefore, two key operational parameters demand prior definition in the

simulation plan, the λ ratio achieved from simulations ranging from 1 to 2 and the engine speed, spanning from 2000 to 5000 rpm.

Afterwards, some other variables and parameters are defined within the simulation software, with particular emphasis on establishing appropriate boundary conditions. The boundary system encompasses inlet, outlet, and wall boundaries. Thus, beginning with the inlets, which includes the "Air Inlet", the main parameters have been compiled in Table 3 of previous experiments carried out by Ortiz-Imedio et al. [29].

In the case of the air inlet, it is important to highlight the pressure and temperature effects related to the engine speed. Regarding the pressure, the higher the engine speed, the lower the pressure used to feed the intake manifold, because when the speed increases, the piston creates a greater vacuum inside of the cylinder, reducing the pressure in the manifold. In parallel with a decrease in intake temperature upon an increase in engine speed, a corresponding drop in pressure occurs due to elevated air flow velocity. This results in lower residence time of air within the intake manifold, consequently limiting the time available for air to warm up. In this context, the outlet system consists of a single boundary condition, called the "Exhaust" condition. Thus, the "Exhaust" condition only requires an outlet pressure definition, which should be set to atmospheric pressure.

Finally, relating to the boundary conditions of the wall systems, these have a strong dependency on the wall temperature, being very closely related to the heat transfer phenomena. In this sense, Table 4 summarizes the wall boundary conditions implemented in the simulations, which were based on diverse literature sources.

As can be observed, several wall boundaries are unaffected by changes in the type of injection since they are not involved in the modified parts or in combustion reaction, and hence, they have been defined with values obtained in PFI experimental bench by our research group, keeping both systems comparable [29].

On the other hand, the walls located in the combustion cylinder region such as piston, head and liner, must be modified in comparison with PFI, in order to get a more realistic result which have been changed to the values reported in literature for DI engines [11]. Moreover, in the case of the liner, similar temperature as head is assumed.

In this sense, ANSYS Forte assumes that the heat flux through the cylinder is mainly produced as consequence of gas-phase convection, fuel-film conduction and radiation [38]. However, the temperature alongside the wall is undertake as a constant, without spatial variation, being all of them configured with the Law of the Wall slip condition for the shear stress to accurately capture wall boundary layer's effect [29,38].

Furthermore, it is necessary to incorporate the defined profiles for the valve opening and closing movements, which are synchronized with the piston strokes, SA and SOI timings.

At this point, the main feature for modelling this type of injection on ANSYS Forte compared with PFI simulations is the Forte spray model, which allows to reproduce the injection of fuel. Afterwards, the DI 5-nozzle configuration is selected to be implemented in ANSYS Forte since it is a widely used layout and easy to reproduce. To achieve this, the dispensed jets from each injector nozzle must be modelled, being indispensable to give the exit position and the polar and cylindrical coordinates defining their trajectory, as can be seen in Fig. 2.

Additionally, simulation time is saved by assessing a single engine cylinder. This simplifies the simulation and power extrapolation for the 4-cylinder engine, assuming that each cylinder is geometrically identical.

Table 3
Air inlet critical boundary conditions: Pressure and Temperature [29].

Air Inlet		
Speed (rpm)	**Pressure (bar)**	**Temperature (K)**
2000	0.92	314
3000	0.91	311
4000	0.89	309
5000	0.88	307

Table 4
Walls boundary conditions: Wall temperature (K).

Boundary Condition	Temperature (K)	References
Piston	570	[11]
Head	550	[11]
Liner	550	–
In Valve	400	[9]
Out Valve	550	[9]
Intake Manifold	313	[9]
Exhaust Manifold	500	[9]

Finally, to summarize all the steps to carry out the simulation and the modelling test points, a general outline is depicted in Fig. 3.

In this sense, ANSYS Forte solves different equations such as fluid continuity, momentum and energy conservation and gas-phase mixture equation of state through different models to carry out several purposes. The explained combustion model GRI-Mech 3.0 includes all the feasible reactions with all the fuels assessed in this study, even the formation of NOx. In addition, the turbulent flow model used in this study was the Reynolds-Averaged-Navier-Stokes (RANS) Re-Normalization Group (RNG) k-ε model.

Finally, regarding the spray model selected, the droplet collision model is based on the adaptive collision mesh model and the solid-cone injection is initialized with the nozzle-flow model, which offers a description about nozzle discharge characteristics. This nozzle-flow model describes the instantaneous flow conditions inside the nozzle. Furthermore, unsteady gas jet model is employed in order to reduce the mesh-dependency of the Kevin-Helmholtz/Rayleigh-Taylor (KH-RT) breakup model [38].

2.3. Simulation plan

Thereafter, the simulation plan requires meticulous definition of the injection velocity (v_i) and pulse width (PW), deemed as critical operational variables governing the performance and demands of each simulation. These parameters are mathematically represented in Eqs. (3) and (4) [39].

$$v_i = \frac{\dot{m}_f}{\rho_i \cdot A_{Nozzle} \cdot N_{Nozzle} \cdot 100} \tag{3}$$

$$PW = \frac{N \cdot m_{full}}{\dot{m}_f} \tag{4}$$

Where $\dot{m}_f$ is the mass fuel inlet flow (g/s), ρ_i is the density at atmospheric conditions (g/cm^3), A_{Nozzle} is the cross-section of the nozzle (cm^2), N_{Nozzle} is the number of nozzles, N is the engine speed (rpm), $\dot{m}_f$ is the mass flow of fuel injected per cycle $\left(\frac{g}{s}\right)$ and m_{full} is the total mass of fuel injected per cycle (g).

Finally, the simulation plan contains the values of λ obtained from Eq. (1) for each engine speed (rpm), the SA (dBTDC), v_i (m/s), PW (CAD), $\dot{m}_f$ (g/s), the injection pressure (P_{Inj}) and the SOI and EOI, presented in Table 5, comparing analogous experiences between DI and PFI.

In this study the simulations were executed in a workstation which uses a message passing interface (MPI) solver with two processors Intel® Xeon® Gold 6148 of 20 physical cores each one and 256 GB of RAM. Furthermore, to maximize the efficiency of the simulation workflow a Python script to post-process the ANSYS Forte results has been developed.

2.4. Engine performance basis

Low carbon fuel performance was compared at optimum SA and

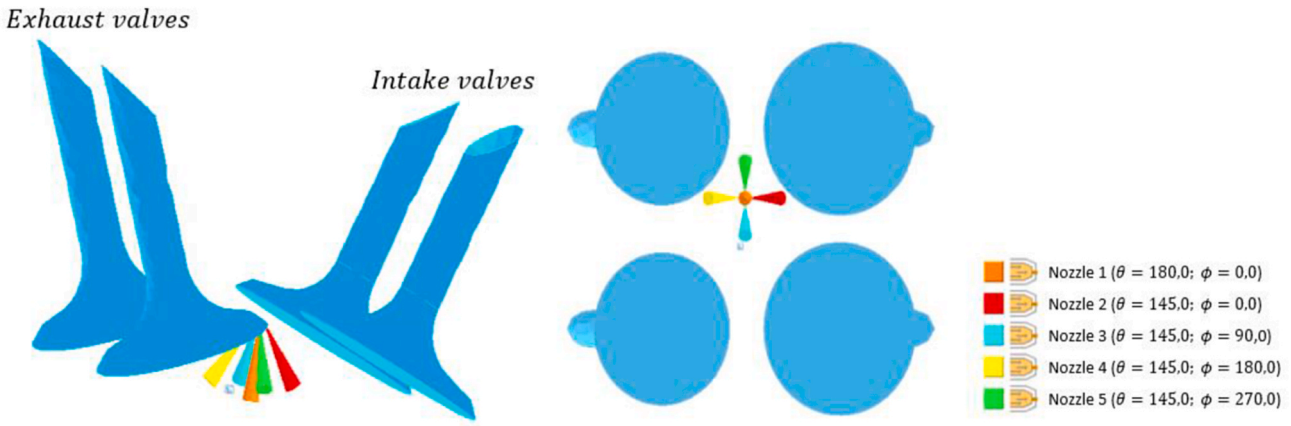

Fig. 2. Spray injection geometry at the simulation model.

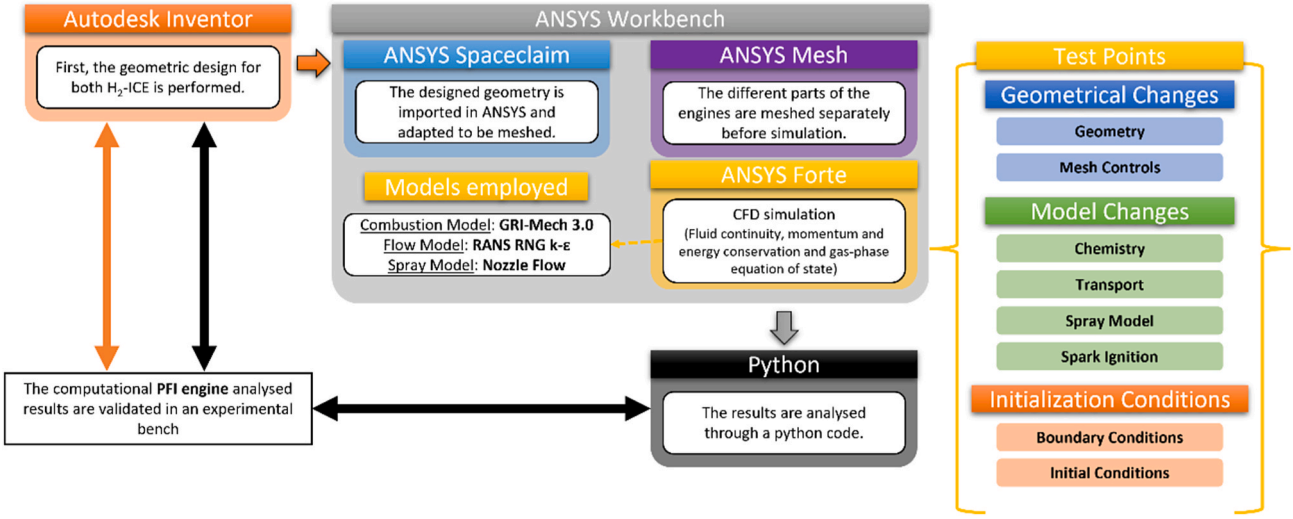

Fig. 3. General simulation procedure.

Table 5
Simulation plan.

Direct Injection (DI)											
Fuel	λ	RPM	SA (dBTDC)	DI				PFI			
				P_{Inj} (bar); Vi (m/s)	PW (CAD)	$\dot{m}_f$ (g/s)	EOI (∘)	P_{Inj} (bar); Vi (m/s)	PW (CAD)	$\dot{m}_f$ (g/s)	SOI (∘)
H_2	1.5	2000	10	100; 494	15	5.83	630	3; 275	93	0.30	485
		3000	10		22	5.83	600		150	0.30	490
		4000	15		34	5.83	570		216	0.30	495
		5000	15		43	5.83	540		278	0.30	500
H_2	2	2000	25		12	5.83	630		76	0.30	485
		3000	25		17	5.83	600		120	0.30	490
		4000	25		26	5.83	570		179	0.30	495
		5000	25		33	5.83	540		225	0.30	500
CH_4	1.5	2000	45	100; 207	13	19.43	630	3; 115	69	1.0	485
		3000	60		20	19.43	600		107	1.0	490
		4000	60		31	19.43	570		164	1.0	495
		5000	60		39	19.43	540		201	1.0	500
COG	1.5	2000	25	100; 234	16	13.60	630	3; 150	16	0.7	485
		3000	25		25	13.60	600		25	0.7	490
		4000	25		40	13.60	570		40	0.7	495
		5000	25		49	13.60	540		49	0.7	500

wide-open throttle (WOT) conditions to reach the maximum brake torque (MBT) across all speeds and lambda ratios, using identical initial values. In this context, higher values of λ leads to brake power reduction, and thus, reduced torque. This phenomenon is caused by the lower H_2 concentration in the air-fuel mixture.

Conversely, the higher air mass fosters an increase in volumetric

efficiency (η_e), the key variable to assess the different performance of DI and PFI. This improvement in η_e stems from the elevated O_2 proportion, as consequence of the greater air intake during the admission stroke. For this reason, η_e and the air mass inlet flow ($\dot{m}_e$) are directly correlated, as depicted in Eq. (5) [39].

$$\eta_e = \frac{2 \cdot \dot{m}_e}{\rho_{a,i} \cdot V_d \cdot N} = \frac{m_a}{\rho_{a,i} \cdot V_d} \tag{5}$$

Where $\rho_{a,i}$ is the air density at atmospheric conditions (g/cm^3), $\dot{m}_e$ is the air mass inlet flow (g/h) and m_a is the real air mass entering into the cylinder (g).

The selected parameters to characterize the engine performance, power (P), brake mean effective pressure (BMEP) and torque are described by the following expressions presented in Eqs. (6), (7)and (8) [39].

$$P = \frac{W_{c,i} \cdot N}{\eta_R} = 2 \cdot \pi \cdot N \cdot T \cdot 10^{-3} \tag{6}$$

$$BMEP = \frac{P \cdot \eta_R}{V_d \cdot N} = \frac{W_{c,i}}{V_d} \tag{7}$$

$$W_{c,i} = \oint p \cdot dV \tag{8}$$

Where η_R is the number of crank revolutions for each power stroke per cylinder ($\eta_R = 2$), $W_{c,i}$ is the work delivered per cycle (J/Cycle), V_d is the cylinder volume displaced by the piston in all the cylinders (dm^3), p is the pressure obtained during compression stroke (bar) and N is the engine speed (rev/s).

The relationship between power and volumetric efficiency stems from power density. The displacement volume effect arises from the higher density of the air compared to H_2. When H_2 is injected into an intake air stream, its lower density relative to air leads to occupy a greater volume in a certain physical space, displacing some of the surrounding air and hindering the entry into the combustion cylinder.

On the other hand, after adaptation to DI, the full air stream is introduced, followed by DI of H_2 when inlet valve is completely closed, increasing the amount of air-fuel mixture per cm^3 of cylinder volume for the same λ, promoting the volumetric efficiency. Nevertheless, H_2 is injected at higher pressure (100 bar) than the injection pressure in PFI (3 bar), requiring prior fuel energization. The high injection pressure of 100 is selected as high-speed flow injectors in DI generally requires this level of pressure to reach the instantaneous flow with H_2 [30,42].

However, a primary drawback of this approach is a less stratified mixture, which could negatively impact combustion efficiency, brake-specific fuel consumption, and NOx emissions.

In this way, torque represents the rotational force generated by the engine, produced after combustion during the expansion stroke. The release of chemical heat leads to torque generation, which is subsequently converted into power. Additionally, BMEP measures engine efficiency, defined as the mean effective pressure exerted over the piston and developed during combustion. As a result, both variables are crucial to evaluate engine performance, serving as a reference of the extent to which the various forces exerted as a consequence of the combustion reaction in an ICE are utilized.

Furthermore, the engine performance, especially in H_2-ICEs, apart from the widely known parameters of power, torque and BMEP, must be also assessed in terms of BTE and brake specific fuel consumption (BSFC), related to peak temperatures reached during combustion stroke and the specific nitrogen oxides emission levels (sNOx), most of them directly or inversely related with brake power and chemical heat release (CHR), as it was defined in Eqs. (9), (10) and (11) [39].

$$BTE = \frac{W_c}{m_f \cdot LHV} = \frac{\left(\frac{P \cdot \eta_R}{N}\right)}{\left(\dot{m}_f \cdot \frac{\eta_R}{N}\right) \cdot LHV} = \frac{1}{BSFC \cdot LHV} \tag{9}$$

$$sNOx = \frac{\dot{m}_{NOx}}{P} \tag{10}$$

$$CHR = H_R(T_A) - H_P(T_A) \tag{11}$$

Where $\dot{m}_f$ is the mass flow of fuel injected per cycle (g/s), LHV is the lower heating value in mass base (J/g), $\dot{m}_{NOx}$ is the mass flow of generated NOx, H_R is the reagent enthalpy (J) and H_P the product enthalpy (J), both of them at ambient temperature (T_A) (K).

Finally, regarding NOx formation, which is commonly found in H_2 combustion, this process is primarily governed by temperature, according to the extended Zeldovich reaction model [40]:

$$N_2 + O \leftrightarrow NO + N$$

$$N + O_2 \leftrightarrow NO + O$$

$$N + OH \leftrightarrow NO + H$$

3. Results and discussion

This section presents the major outcomes derived from the simulations that compare the performance of DI and PFI engines in terms of brake power, torque, BMEP, thermal and volumetric efficiencies, specific fuel consumption, heat release and sNOx emissions. In addition, the analysis also assesses the potential of the different low carbon fuels used in both engines, particularly focusing on H_2.

3.1. Hydrogen engines performance comparison: DI vs PFI

3.1.1. Engine performance

First, the maximum pressure reached during combustion exhibits the power delivered. In this case, the pressure curves for H_2 at different engine speeds and λ ratios of both engines are shown in Fig. 4.

In H_2 simulations, peak pressure was measured at engine speeds from 2000 rpm to 5000 rpm and λ ratios of 1.5 and 2. According to the results obtained, higher λ drives a peak pressure reduction as a consequence of lower enriched air-fuel mixtures. Conversely, peak cylinder pressure increases with engine speed (rpm). In this respect, it is important to highlight that both engines have been reproduced using the same spark advance (SA) on each simulation experience, varying in the same proportion based on λ factor.

Thus, in the case of PFI, working at λ = 1.5 and 5000 rpm results in a peak pressure of 65.4 bar, while DI obtains 79.4 bar. Consequently, peak pressure fuelling H_2 at optimum λ (λ = 1.5) is among 8.7–21.4% higher using DI than PFI at different engine speeds.

Furthermore, this figure illustrates the disparity in SA between simulations conducted at λ = 1.5 and λ = 2 in both engines. In this context, simulations at λ = 2 exhibit an advancement of 15 crank angle degrees (CAD) compared to λ = 1.5 simulations. Consequently, when operating under leaner conditions (λ = 2), the combustion reaction initiates earlier, and the pressure peak is reached close to the top dead centre (TDC), resulting in a smoother slope on the curve. On the other hand, conducting simulations at the optimal air-fuel ratio (λ = 1.5) portrays a steeper slope, from 710 CAD at 2000–3000 rpm and 705 CAD at 4000–5000 rpm. This abrupt increase means that the combustion reaction occurs in less time than under leaner conditions as consequence of the higher flame temperature generated, which promotes the laminar flame speed (S_L), leading to higher pressure peaks. Therefore, a more efficient combustion reaction with a faster release of energy and higher combustion temperatures is achieved.

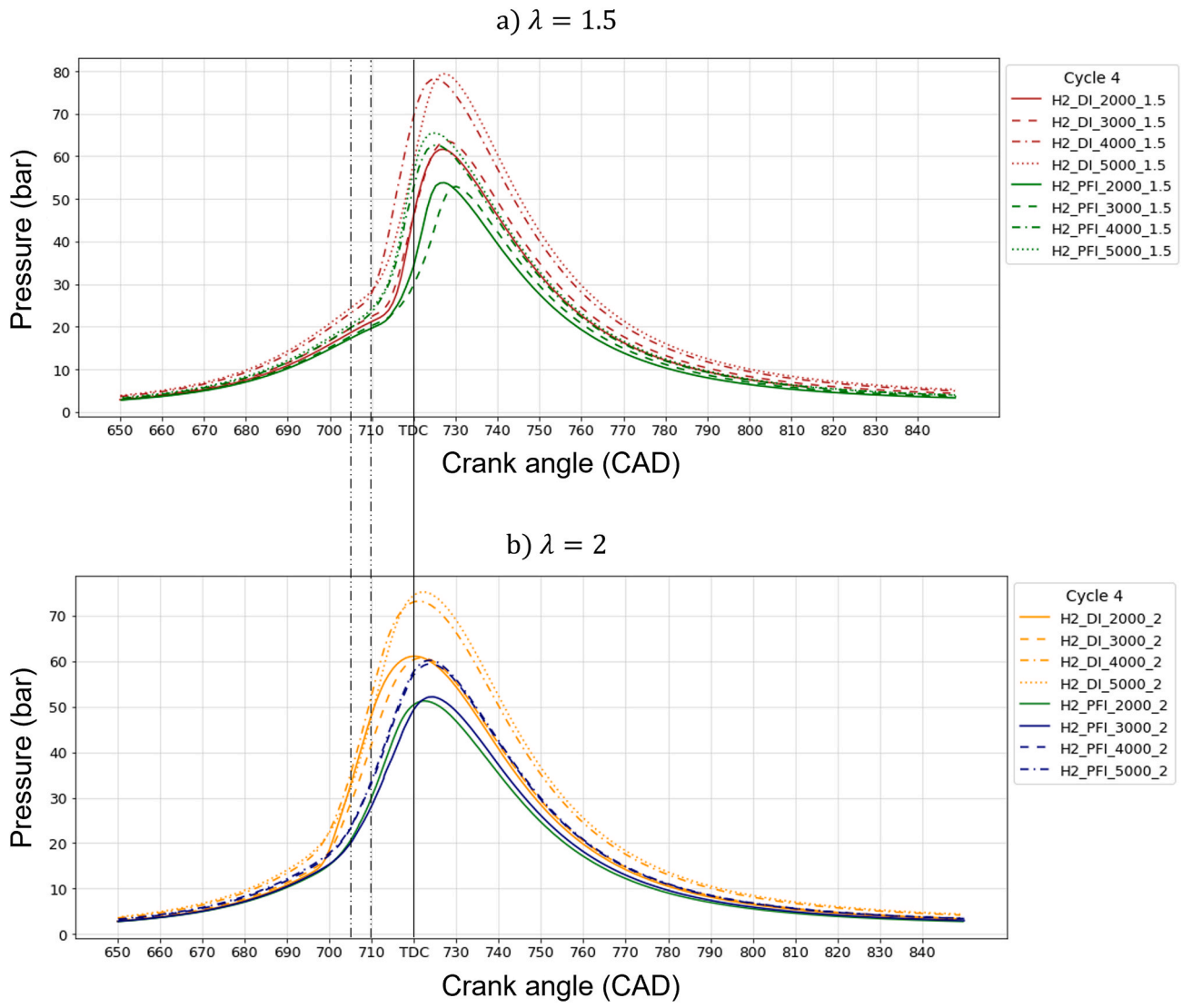

Fig. 4. H_2 -ICE pressure analysis during combustion at different air-fuel ratios a) $\lambda = 1.5$ and b) $\lambda = 2$.

It is worth noting that there is a direct relationship between pressure and power which also affects to torque and BMEP by means of $W_{c,i}$. The higher peak pressure in DI is enabled by the enhancement in volumetric efficiency as consequence of a better distributed and homogeneous mixture inside the cylinder, which increases the power density. However, the increase in pressure leads to a simultaneous increase in temperature, promoting the formation of thermal NOx.

In this context, Fig. 5 presents the key engine performance metrics, encompassing brake power depicted as lines, volumetric efficiency represented as columns, torque and BMEP, which are influenced by engine speed (rpm) and λ ratio.

In this case, simulations conducted at optimal air-fuel ratio (Fig. 5a, $\lambda = 1.5$) reveal a notable discrepancy in volumetric efficiency between PFI and DI, ranging from 18.3% to 30.6% higher in the case of DI. This difference persists across the entire engine speed range, correlating with a corresponding power increase between 27.3% and 39.5%. The observed difference among type of engines arises as a result of the displacement volume effect. In PFI configuration, the process impedes air intake due to the lower density of H_2, requiring a larger volume per mass unit. Consequently, a reduced quantity of air-fuel mixture is introduced to attain the desired λ ratio, and hence, control over the dosage is more complex. This leads to a decline in power density and simultaneously a decrease in the released energy while combustion is taking place.

Accordingly, an increase in engine speed conducts to greater intake and expulsion of the air-fuel mixture, resulting in combustion reactions that generate more thermal energy in each cycle. As a result, higher engine speeds yield more power. Furthermore, this leads to an enhanced volumetric efficiency using DI configuration, which ranges from 73.6% to 93.1% and a brake power that ranges from 4.2 kW to 12.8 kW within that engine speed range for just one cylinder analysed. Consequently, considering the 4-cylinder engine configuration, an approximately 11 kW more powerful engine is obtained adapting the configuration from PFI to DI, assuming a total increase of 14.8 horse power (HP).

Conversely, simulations performed under leaner conditions (Fig. 5b, $\lambda = 2$), yield lower performance as less air is introduced per cycle, thereby reducing the available energy during combustion. However, in case of DI, compared to optimal air-fuel ratio (Fig. 5a, $\lambda = 1.5$), volumetric efficiency remains unaffected since the amount of air introduced keeps constant while fuel mass is reduced. On the other hand, in PFI configuration, under leaner conditions, as consequence of the lower amount of fuel injected, a higher amount of air is introduced inside of the cylinder enhancing volumetric efficiency, although the lower fuel concentration in mixture causes a power output detriment. Consequently, brake power decreases when operating at $\lambda = 2$ compared to $\lambda = 1.5$. Specifically, DI delivers among 35.6%–41.4% less power from

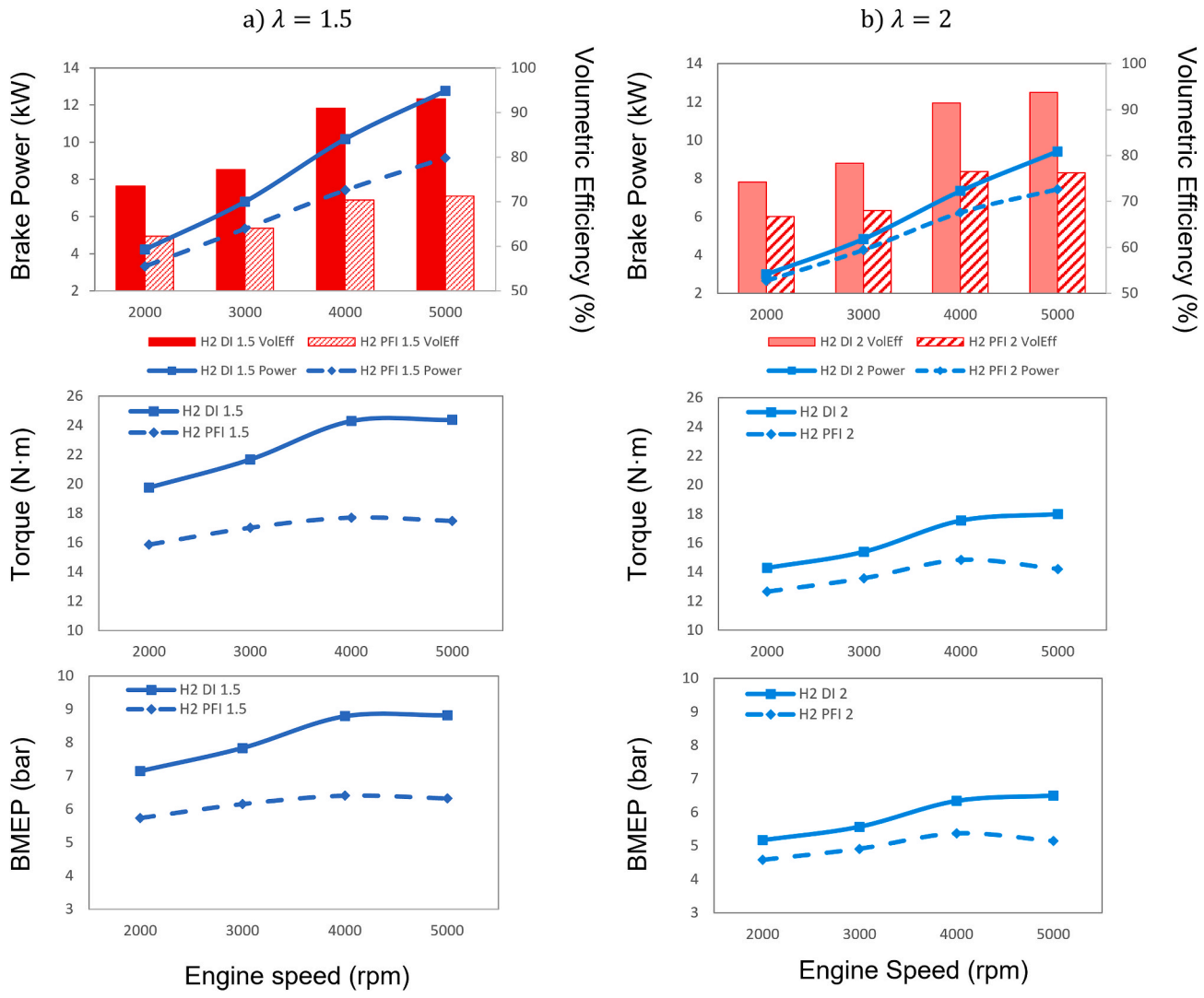

Fig. 5. H_2 engine performance comparison at different air-fuel ratios a) $\lambda = 1.5$ and b) $\lambda = 2$.

2000 to 5000 rpm, while the PFI engine experiences a reduction from 19.3% to 25.4%.

Thus, DI configuration achieves closer results, in terms of brake power, to the PFI configuration operating at $\lambda = 2$, although there is still a gap between them ranging from 12.8% to 26.5% in favour of DI.

Finally, torque and BMEP are plotted against various engine speeds and air-fuel ratios, operating at $\lambda = 1.5$ (Fig. 5a) and $\lambda = 2$ (Fig. 5b). Under optimal conditions (Fig. 5a, $\lambda = 1.5$), a comparable pattern is noted in both variables, mirroring the trends observed in the brake power results because both are directly related, with torque and BMEP in DI being 27.3%–39.5% greater than PFI. In contrast, under lean conditions (Fig. 5b, $\lambda = 2$), torque and BMEP experienced reductions ranging from 34.9% to 40.7% compared to optimal λ. However, DI configuration results still exhibit a superiority of 12.8%–26.5% over PFI.

3.1.2. Thermal efficiency and emissions

Once engine performance parameters are assessed, as consequence of the higher performance achieved at the optimal air-fuel ratio ($\lambda = 1.5$), this value is predetermined for analysing thermal efficiency and emissions behaviours in both engine configurations.

As illustrated in Fig. 6, the selected variables for describing thermal efficiencies are the chemical heat release (CHR), brake thermal efficiency (BTE) and brake specific fuel consumption (BSFC), which is represented by the blue line. Fig. 6 also depicts, sNOx and maximum combustion temperature reached across the entire range of engine speeds.

In this context, the elevation in engine speed involves an increased chemical heat release (CHR) per cycle due to the growth in the air-fuel mixture introduced. Moreover, brake specific fuel consumption (BSFC) rises despite the power gain as consequence of the higher injection flowrate ($\dot{m}_f$). Therefore, as engine power increases, BTE diminishes as a result of the indirect correlation with BSFC.

In the obtained results, simulation runs at the optimal air-fuel ratio ($\lambda = 1.5$), H_2 attains elevated CHR levels using a DI engine in comparison with PFI configuration. This is attributed to the enhanced capacity of DI to introduce a greater quantity of air-fuel mixture, culminating in higher CHR values, effectively transforming more chemical energy into mechanical energy. Consequently, the utilization of DI instead of PFI leads to percentage increase in CHR ranging from 19.0% to 35.5%, which results in an additional CHR amount of 883.3 J/cycle when considering the entire 4-cylinder engine.

The rise in brake power requires a widening pulse width (PW) as a consequence of the corresponding increase in the amount of fuel mass injected. Thus, BSFC values elevate as engine speed increases. Nevertheless, the lower power output of PFI engines negatively impacts BSFC, despite their lower fuel consumption per cycle compared to DI engines. In this context, DI results in a percentual reduction of BSFC compared to PFI, ranging from 1.4% to 4.8%.

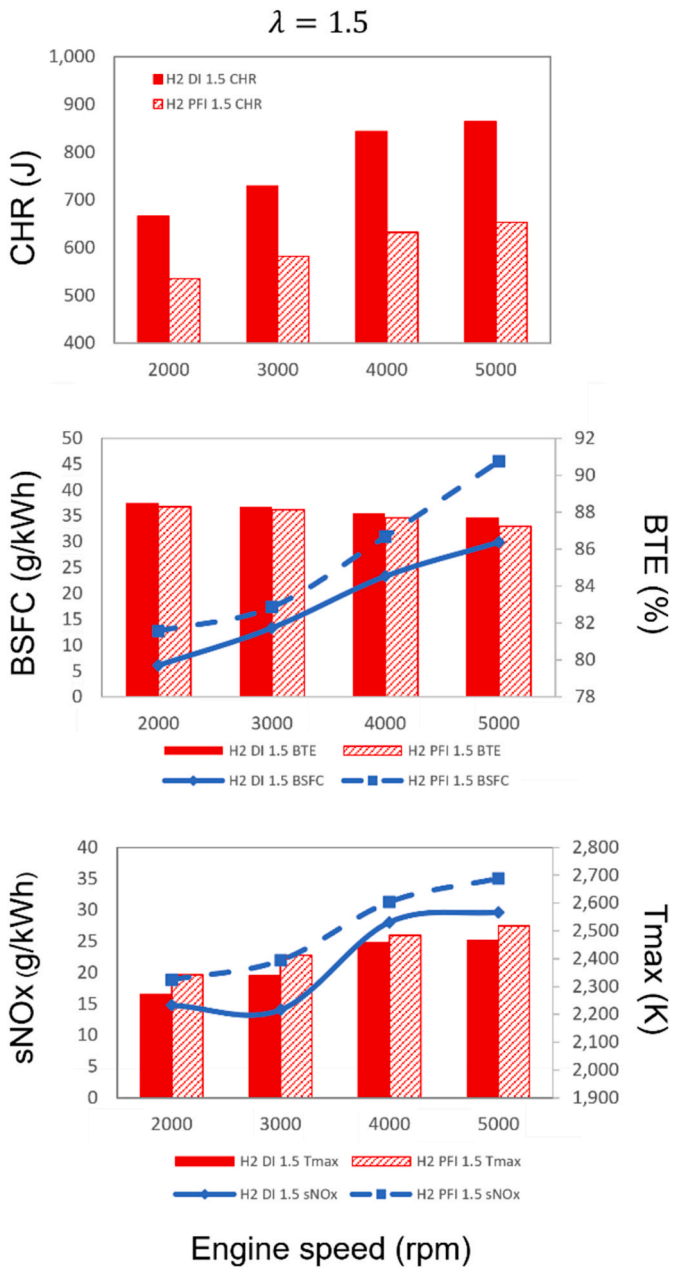

Fig. 6. Heat released, thermal efficiency and NOx emission comparison in H_2 engines.

Conversely, BTE and BSFC display strong interdependency, with brake power significantly influencing them. In this sense, BTE diminishes with the increase in BSFC, stemming from the heightened fuel requirement to generate an equivalent amount of energy, resulting in greater losses. Subsequently, upon analysing the entire range of engine speeds (rpm), the utilization of DI configuration contributes to the increment of BTE between 0.5% and 1.7% compared to PFI. Specifically, H_2 attains a peak BTE of 37.6% and a minimum BSFC of 79.7 g/kWh.

Finally, NOx emissions exhibit a direct proportional relationship with combustion temperature, which increase with the engine speed as consequence of the greater amount of heat released during combustion.

In the DI system, air is introduced before hydrogen injection, reducing the tendency to pre-ignition and also lowering the local in-cylinder temperature, as consequence of H_2 expansion derived from high-pressure direct injection [27]. This leads to the formation of a more homogeneous air-fuel mixture, fostering more efficient and uniform combustion, converting more energy released into useful work instead of remanent heat [41].

Moreover, the reduction of WHT losses leads to better mixing, and hence, the local peak temperatures in the cylinder are reduced [43]. Therefore, an increase in CHR using the DI configuration compared to PFI suggests an increase in useful power, but not a temperature increase, as WHT losses are reduced.

Thus, the maximum temperature reached in DI is reduced between 25.5K and 73.9K, together with a decrease in sNOx ranging from 10.4% to 36.0% compared to PFI. In addition, DI system reaches the minimum levels of sNOx at 3000 rpm (14.06 g/kWh), as consequence of the higher brake power augmentation in comparison with 2000 rpm.

In the PFI configuration, the air excess burns a larger quantity of H_2, which possesses a higher LHV, further elevating the mixture temperature at high engine speeds and subsequently promoting the formation of thermal NOx. For instance, a peak temperature rise of 266.1 K is observed from 3000 rpm to 4000 rpm.

Consequently, it can be concluded that the H_2-ICE DI exhibits superior power output and lower emission levels compared to PFI, under the studied conditions.

3.2. Low carbon fuels performance comparison: DI vs PFI

3.2.1. Engine performance

Ansys® Forte® software enables the assessment of different fuel types, using the same variables and parameters. This facilitates the comprehensive analysis of the performance, including previous H_2 results, and those obtained in CH_4 and COG simulations at ($\lambda = 1.5$). Fig. 7 depicts the comparison of the performance of the three fuels at the H_2 optimal air-fuel ratio ($\lambda = 1.5$) within the entire range of engine speeds (2000–5000 rpm). Thus, brake power, volumetric efficiency, torque and BMEP are assessed for both injection systems.

In PFI configuration (Fig. 7a), the maximum power output achieved is 9.5 kW when utilizing COG at 5000 rpm. The superior brake power observed in COG is attributed to the higher S_L compared to CH_4, leading to higher efficiencies since a more complete combustion is achieved. Conversely, COG has a greater density than H_2 and a substantial amount of energy is delivered during combustion owing to higher volumetric efficiency. In this sense, compared to H_2, brake power increases from 0.9% (+0.1 kW/cyl) to 12.7% (+0.6 kW/cyl), and compared to CH_4 brake power spans from 10.0% (+0.3 kW/cyl) to 30.2% (2.86 kW/cyl) in favour of COG within the entire range of engine speeds.

In addition, the obtained volumetric efficiency is among 7.5%–10.8% greater running COG in PFI engines than H_2. The enhanced volumetric efficiency stems from the higher volumetric density of COG, which is in mass % primarily composed by CH_4. This increased density mitigates the effect of volume displacement at the inlet, leading to gains in volumetric efficiency. Furthermore, COG volumetric efficiency remains lower than CH_4 ranging from 4.7% to 6.7%. The volumetric efficiency of COG reaches the maximum at 4000 rpm, resulting in the highest power difference between fuels. Therefore, PFI system finds a performance limitation on 4000 rpm, reaching almost the same peak pressure as seen in the latter simulation at 5000 rpm while injecting more amount of fuel and reducing the overall efficiency. This limitation is overcome by changing the injection system to DI, which means that DI engine could even work at higher speeds resulting in a performance improvement.

Regarding DI configuration (Fig. 7b), H_2 achieves a maximum power output of 12.8 kW at 5000 rpm. Moreover, H_2 obtains the highest brake power using the DI configuration, even generating a power output 21.9% higher than COG and 78.9% higher than CH_4 both fuelled in DI engines. Thus, CH_4 is greatly disadvantaged while working over the λ_{St}, where CH_4 optimal combustion conditions are normally achieved.

This power enhancement in H_2 combustion simulations is obtained as consequence of the growth of volumetric efficiency. In this context, H_2 exhibits the greatest sensitivity to engine changes in volumetric

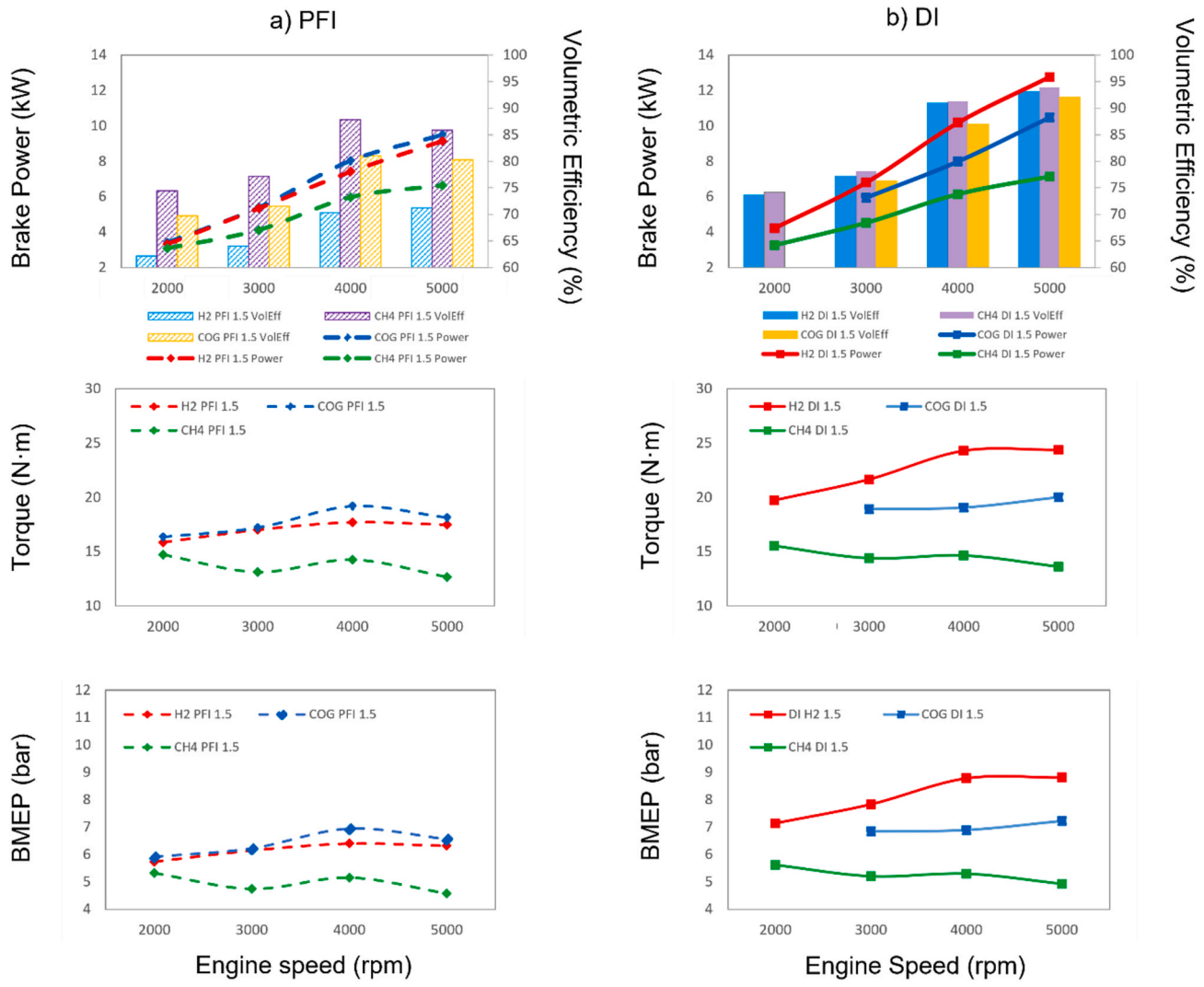

Fig. 7. Low carbon fuels engine performances comparison with different engine configurations a) PFI and b) DI.

efficiency among the analysed fuels. However, in every case the volumetric efficiency is improved, and hence, the brake power. In accordance, H_2 increases volumetric efficiency by 30.6% in the maximum, COG by 14.8% and CH_4 by 9.4%, since H_2 has the lowest density and CH_4 the highest one.

Finally, torque and BMEP follows the same trends as brake power and volumetric efficiency. Accordingly, the maximum torque in the PFI configuration is achieved when employing COG as fuel and operating at 4000 rpm due to the higher brake power reached at this engine speed, generating 19.2 N m and achieving a maximum BMEP of 6.9 bar. In contrast, the DI configuration reaches the maximum torque and BMEP using H_2 at 5000 rpm, resulting in 24.4 N m and 8.82 bar. This means a noteworthy enhancement in conversion efficiency of heat released into useful work, as evidenced by the increase in BMEP values. This improvement indicates a more favourable response in a high-load due to the increased torque, in addition to the greater brake power delivered.

Thus, H_2 is the best fuel compared at the designed DI engine in terms of engine performance with regard to the final results and improvement. Conversely, it is important to highlight that COG is obtained after valorisation of an industrial residual gas stream, although it has intermediate properties between H_2 and CH_4 regarding density, LHV, and S_L.

3.2.2. *Emissions and thermal efficiency*

As illustrated in Fig. 8, the performance and the efficiency are assessed together with the emissions associated with each fuel used in DI and PFI configurations. CHR, wall heat transfer (WHT) and maximum combustion temperature are represented by bars, and, sNOx are represented by trend lines. Finally, the comparison between BTE and BSFC is also illustrated.

Regarding the PFI configuration (Fig. 8a), it is observed that the assessed fuels deliver comparable CHR. However, within this configuration, COG achieves the lowest wall heat transfer (WHT) values at optimal air-fuel ratio ($\lambda = 1.5$). Consequently, H_2 experiences higher wall losses than COG, from 2.9 to 20.3 J/cycle, while CH_4 incurs losses 23.6–70.6 J/cycle above COG levels. This discrepancy in WHT contributes to COG and H_2 showing significantly higher brake power than CH_4, because more heat is converted into useful work, even though CHR is similar and lower combustion temperatures are achieved. In the case of CH_4, this effect occurs due to the negative work generated as consequence of reaching the pressure peak before the TDC, while piston keeps compressing and reducing the effective work.

In light of the above, the elevated combustion temperatures during CH_4 combustion, foster the formation of thermal NOx, resulting in the highest observed sNOx levels. In contrast, the mitigating effect of CH_4 when mixed with H_2 leads to a reduction in sNOx emissions during COG combustion, showcasing reductions ranging from 31.9% to 111.6% compared to H_2. In this sense, CH_4 results in higher combustion temperatures but also in greater WHT, as consequence of the lower BTE.

Regarding efficiency, within the PFI configuration, H_2 is emerging as the fuel with the minimum energy consumption for power generation,

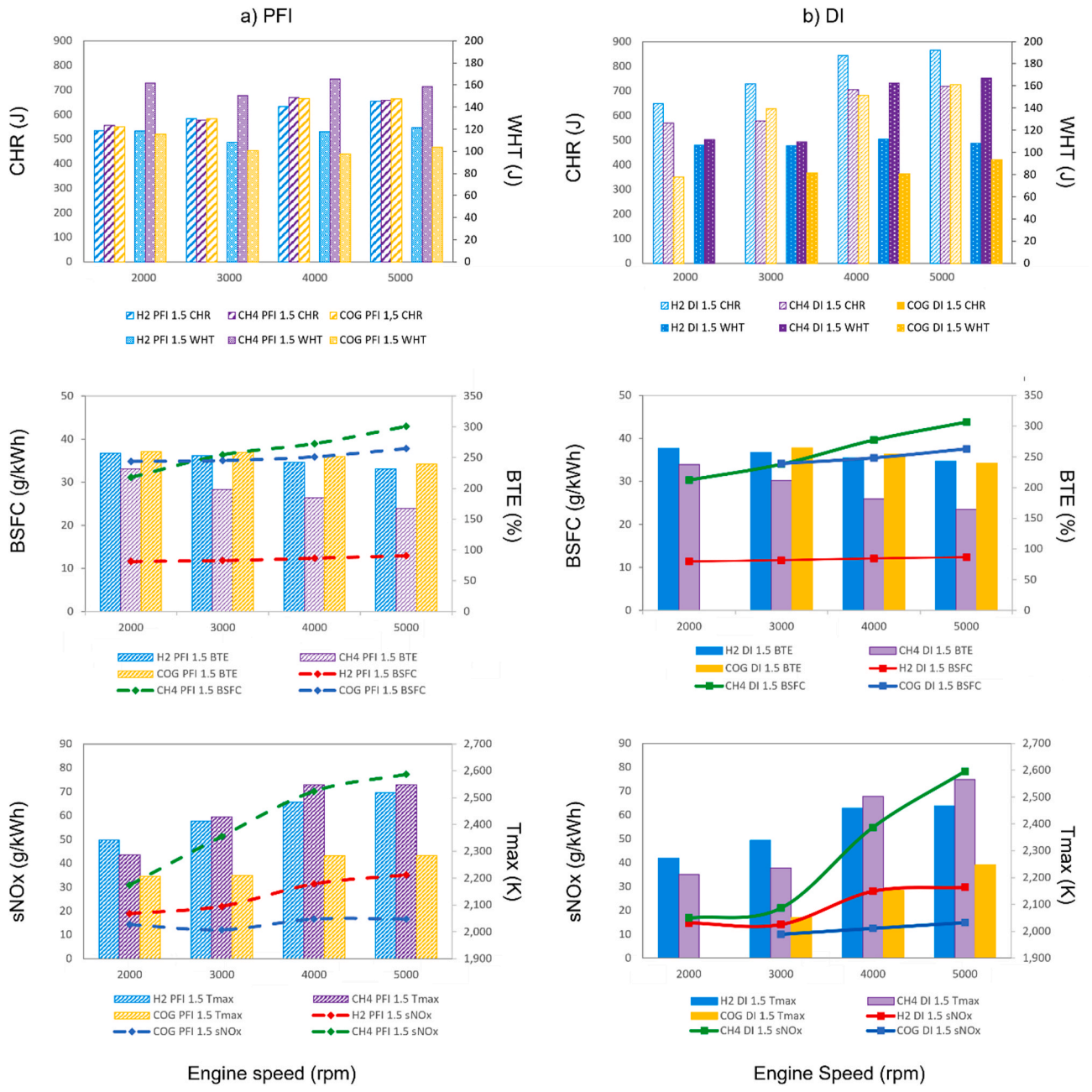

Fig. 8. Performance, efficiency and sNOx emissions comparison in low carbon fuels with different engine configurations a) PFI and b) DI.

also manifests a high thermal efficiency similar to the COG. Furthermore, relating to BSFC, H_2 exhibits values between 65.5%-66.5% and 62.5%–69.9% lower values than COG and CH_4, respectively.

In DI simulations (Fig. 8b) working under identical conditions ($\lambda = 1.5$), since H_2 obtains the highest power output, it also releases the greatest amount of chemical heat, exceeding the CHR obtained for the COG at the same λ between 16.4% and 28.8% and showing the higher chemical combustion potential of H_2 compared to other fuels.

Moreover, when simulating within this injection system, COG presents intermediate results between H_2 and also CH_4 for DI. This results in an improvement of CHR by 9.4% at maximum engine speed after enhancing the volumetric efficiency of the air-fuel mixture through the transition from PFI to DI configuration.

However, the combustion of H_2 results in greater energy losses through the walls, that exceed of those of COG by 4.2–25.7 J/cycle, and CH_4 also experiences losses from 8.7 to 65.3 J/cycle above COG. In addition, when compared to PFI, the WHT for H_2 is reduced from 2.0% to 10.9%, COG spans from 10.2% to 19.1% and for CH_4 from 0.9% to 28.7%. This reduction in thermal losses is attributed to the improved combustion reaction facilitated by DI strategies, mitigating the effect of incomplete reaction zones that release inefficient heat.

In the case of sNOx, emission levels increase considerably at high speeds, reaching in CH_4 simulations a value of 78.3 g/kWh that is almost twice the sNOx emissions of DI H_2 at 5000 rpm.

In the case of H_2 simulations, the maximum emissions value is 29.6 g/kWh, representing a reduction of 62.1% in sNOx compared to CH_4. However, this value is 55.7% higher than the emissions generated using COG. Consequently, the inclusion of a mixture of CH_4 and H_2, represented in COG simulations exhibits NOx-reducing properties, achieving the lowest sNOx levels of the three, even at maximum engine speed, measuring 14.9 g/kWh at 5000 rpm. Additionally, COG reduces the maximum combustion temperature in the range of 219.0 K–305.0 K

compared to H_2.

Therefore, DI systems contributes to reduce sNOx emission levels in all scenarios. In summary, DI reduces sNOx emissions 7.9 g/kWh for H_2 at 3000 rpm, 4.2 g/kWh for COG at 4000 rpm and 30.3 g/kWh for CH_4 at 3000 rpm, compared to PFI.

Finally, regarding BTE and BSFC, H_2 achieves the best values, similar in DI and PFI configurations. However, H_2 reduces BSFC in the range of 62.4%–71.8% compared to CH_4 and 65.8%–67.2% compared to COG. In terms of BTE, both H_2 and COG achieve comparable results. However, H_2 consistently outperforms CH_4 by a margin of 3.7%–11.3%. This superiority stems from the exceptional calorific power per unit mass of H_2 and remarkable thermal efficiencies, which facilitate a more efficient energy potential conversion. Therefore, despite the need for high compression of H_2 to achieve autonomy, H_2 remains the preferred choice of fuel, specially achieved in DI engines.

4. Conclusions

In this work a comparative simulation study of the engine performance in DI and PFI has been carried out, both adapted to be fuelled by different low carbon fuels H_2, CH_4 and COG. The simulation model has been developed based on a naturally aspirated Volkswagen Polo 1.4 L SI engine. Thus, simulations were focused on two main parameters with influence on engine performance, air-fuel ratio (λ = 1-2) and engine speed (2000–5000 rpm).

Regarding H_2 simulations, the main conclusions drawn are.

- A CFD model was developed for DI H_2-ICE, showing a performance improvement. Simulations reveal that working under optimal air-fuel ratio conditions (λ = 1.5), the DI H_2-ICE model increases a brake power by 39.5% and the volumetric efficiency by 30.6% compared to the PFI system. These findings corroborate the detrimental effect of volume displacement on engine performance, a characteristic limitation of PFI gas fuel combustion systems. On the other hand, torque and BMEP increases in the same proportion.
- Concerning sNOx emissions, the DI offers a prominent NOx-reduction potential, emitting a maximum of 29.6 g/kWh, which suppose a 36% reduction compared to PFI. This reduction is achieved through the lower value of the maximum temperature reached and the higher power delivered which is inversely proportional to sNOx.
- Using DI configuration, H_2 attains a peak BTE of 37.6% and a minimum BSFC of 79.7 g/kWh, performing better than PFI. In addition, the utilization of DI instead of PFI leads to a 35.5% more energy released, which results in an additional CHR amount of 883.3 J/cycle when considering the entire 4-cylinder engine.
- Leaner H_2 mixtures (λ = 2) experience lower combustion pressures and temperatures, leading to reduced performance. Specifically, DI delivers among 35.6%–41.4% less power.

On the other hand, comparing the performances obtained by different fuels.

- H_2-DI simulations running at the optimum air-fuel ratio (λ = 1.5) show the best engine performance, generating a power output 21.9% and 78.9% higher than COG and CH_4 respectively. In these cases, simulations present the same differences in torque and BMEP.
- COG exhibits the lower sNOx levels since the mixture H_2–CH_4 greatly reduces NOx while keeping good performances. However, H_2-DI configuration still reduces the sNOx levels by 62.1% compared to pure CH_4 at λ = 1.5.
- Regarding BSFC, the H_2-DI combination at $\lambda = 1.5$ achieves the most favourable performance. Thus, H_2 is the more efficient option resulting in a reduction of 71.8% in BSFC compared to CH_4 and 67.2% compared to COG at the same operating conditions, due to the higher LHV per mass unit.
- BTE is very similar in COG and H_2 simulations in both injection systems, while CH_4 achieves the lowest values, losing big amounts of thermal energy during combustion in excess of air.

These findings underscore the necessity of further research on DI H_2-ICEs, considering the evident improvements in engine performance and the high levels of efficiency achieved. DI H_2-ICEs demonstrate competitiveness not only with dedicated H_2 engines but also with other low carbon fuels and even gasoline engines in terms of power output and emissions generation. Moreover, DI technology offers ease of implementation compared to other technologies and the ability to employ synthetic fuels or even fuels recovered from waste streams such as COG. These advantages position DI engines as frontrunner in the decarbonization of road transport.

CRediT authorship contribution statement

Fabián Musy: Data curation, Formal analysis, Investigation, Methodology, Software, Writing – original draft. **Rafael Ortiz:** Conceptualization, Investigation, Methodology, Software, Supervision. **Inmaculada Ortiz:** Funding acquisition, Investigation, Supervision. **Alfredo Ortiz:** Conceptualization, Data curation, Formal analysis, Funding acquisition, Investigation, Methodology, Supervision, Writing – original draft, Writing – review & editing.

Declaration of competing interest

The authors declare that they have no known competing financial interests or personal relationships that could have appeared to influence the work reported in this paper.

Acknowledgement

This research was supported by the European Project HYLANTIC EAPA_204/2016, which is co-financed by the European Regional Development Fund (ERDF) in the framework of the INTERREG ATLANTIC program. The Spanish Ministry of Science and Innovation is also supporting this investigation through the projects PID2021-123120OB-I00, TED2021-129951B–C21, and “Complementary Plan for Energy and Renewable Hydrogen” additionally supported with funding from European Union NextGenerationEU (PRTR-C17. I1) and by Comunidad Autónoma de Cantabria.

References

[1] European Commission. The European Green Deal 2019;53(9):24 [Online] Available: EUR-Lex - 52019DC0640 - EN - EUR-Lex (europa.eu).
[2] Sens M, Danzer C, von Essen C, Brauer M, Wascheck R, Seebode J, Kratzsch M. Hydrogen Powertrains in competition to fossil fuel based internal combustion engines and battery electric powertrains. Environ Sci Eng 2021 [Online] Available: Muster einer ersten Seite (iav.com).
[3] Karagöz Y, Balcı Ö, Köten H. Investigation of hydrogen usage on combustion characteristics and emissions of a spark ignition engine. Int J Hydrogen Energy 2019;44(27):14243–56. https://doi.org/10.1016/j.ijhydene.2019.01.147.
[4] Al-Baghdadi M. An Overview of Hydrogen as an Alternative Fuel Experimental and numerical investigation of the dynamic characteristics of laminated composite plate hybrid with steel View project PEM Fuel Cells R&D View project. 2020 [Online] Available: An Overview of Hydrogen as an Alternative Fuel | Encyclopedia MDPI.
[5] Verhelst S, Sierens R, Verstraeten S. A critical review of experimental research on hydrogen fueled SI engines. SAE Int. J. Engines 2006;115:264–74. https://doi.org/10.4271/2006-01-0430.
[6] Karim GA. Hydrogen as a spark ignition engine fuel. Int J Hydrogen Energy 2003;28:569–77. https://doi.org/10.1016/S0360-3199(02)00150-7.
[7] Dimitriou P, Tsujimura T. A review of hydrogen as a compression ignition engine fuel. Int J Hydrogen Energy 2017;42(38):24470–86. https://doi.org/10.1016/j.ijhydene.2017.07.232.
[8] Stępień Z. A comprehensive overview of hydrogen-fueled internal combustion engines: achievements and future challenges. Energies 2021;14(20):6504. https://doi.org/10.3390/en14206504.
[9] Ortiz-Imedio R, Ortiz A, Urroz JC, Diéguez PM, Gorri D, Gandía LM, Ortiz I. Comparative performance of coke oven gas, hydrogen and methane in a spark

ignition engine. Int J Hydrogen Energy 2021;46(33):17572–86. https://doi.org/10.1016/j.ijhydene.2019.12.165.
[10] Boretti A. Hydrogen internal combustion engines to 2030. Int J Hydrogen Energy 2020;45(43):23692–703. https://doi.org/10.1016/j.ijhydene.2020.06.022.
[11] Yang Z, Zhang F, Wang L, Wang K, Zhang D. Effects of injection mode on the mixture formation and combustion performance of the hydrogen internal combustion engine. Energy 2018;147:715–28. https://doi.org/10.1016/j.energy.2018.01.068.
[12] Kosmadakis GM, Rakopoulos CD, Demuynck J, De Paepe M, Verhelst S. CFD modeling and experimental study of combustion and nitric oxide emissions in hydrogen-fueled spark-ignition engine operating in a very wide range of EGR rates. Int J Hydrogen Energy 2012;37(14):10917–34. https://doi.org/10.1016/j.ijhydene.2012.04.067.
[13] Duan J, Liu F, Yang Z, Sun B, Chen W, Wang L. Study on the NOx emissions mechanism of an HICE under high load. Int J Hydrogen Energy 2017;42(34):22027–35. https://doi.org/10.1016/j.ijhydene.2017.07.048.
[14] Diéguez PM, Urroz JC, Sáinz D, Machin J, Arana M, Gandía LM. Characterization of combustion anomalies in a hydrogen-fueled 1.4 L commercial spark-ignition engine by means of in-cylinder pressure, block-engine vibration, and acoustic measurements. Energy Convers Manag 2018;172:67–80. https://doi.org/10.1016/j.enconman.2018.06.115.
[15] Verhelst S, Maesschalck P, Rombaut N, Sierens R. Increasing the power output of hydrogen internal combustion engines by means of supercharging and exhaust gas recirculation. Int J Hydrogen Energy 2009;34(10):4406–12. https://doi.org/10.1016/j.ijhydene.2009.03.037.
[16] Faizal M, Chuah LS, Lee C, Hameed A, Lee J, Shankar M. Review of hydrogen fuel for internal combustion engines: towards Carbon-Free Combustion. J. Mech. Eng. Res. Dev 2019;42(3):36–46. https://doi.org/10.3390/app9224842.
[17] Tang X, Kabat DM, Natkin RJ, Stockhausen WF, Heffel J. Ford P2000 hydrogen engine dynamometer development. SAE Int. J. Engines 2002. https://doi.org/10.4271/2002-01-0242.
[18] Eichlseder H, Wallner T, Freymann R, Ringler J. The potential of hydrogen internal combustion engines in a future mobility scenario. SAE Int. J. Engines 2003. https://doi.org/10.4271/2003-01-2267.
[19] Shinde BJ, Karunamurthy K. Recent progress in hydrogen fuelled internal combustion engine (H2ICE) - a comprehensive outlook. Mater Today Proc 2022;51:1568–79. https://doi.org/10.1016/j.matpr.2021.10.378.
[20] Matthias NS, Wallner T, Scarcelli R. A hydrogen direct injection engine concept that exceeds U.S. DOE light-duty efficiency targets. SAE Int. J. Engines 2012;5(3):838–49. https://doi.org/10.4271/2012-01-0653.
[21] Mohammadi A, Shioji M, Nakai Y, Ishikura W, Tabo E. Performance and combustion characteristics of a direct injection SI hydrogen engine. Int J Hydrogen Energy 2007;32(2):296–304. https://doi.org/10.1016/j.ijhydene.2006.06.005.
[22] Oikawa M, Ogasawara Y, Kondo Y, Sekine K, Takagi Y, Sato Y. Optimization of hydrogen jet configuration by single hole nozzle and high-speed laser shadowgraphy in high pressure direct injection hydrogen engines. SAE Int. J. Engines 2011. https://doi.org/10.4271/2011-01-2002.
[23] Yip HL, Srna A, Chun Yin Yuan A, Kook S, Taylor RA, Heng Yeoh G, Medwell PR, Nian Chan Q. A review of hydrogen direct injection for internal combustion engines: towards carbon-free combustion. Appl Sci 2019;9(22):4842. https://doi.org/10.3390/app9224842.
[24] Nakagawa K, Yamane K, Ohira T. Potential of large output power, high thermal efficiency, near-zero NOx emission, supercharged, lean-burn, hydrogen-fuelled, direct injection engines. Energy Proc 2012;29:455–62. https://doi.org/10.1016/j.egypro.2012.09.053.
[25] Klepatz K, Rottengruber H, Zeilinga S, Koch D, Prümm W. Loss analysis of a direct-injection hydrogen combustion engine. SAE Int. J. Engines 2018. https://doi.org/10.4271/2018-01-1686.
[26] Nemati A, Fathi V, Barzegar R, Khalilarya S. Numerical investigation of the effect of injection timing under various equivalence ratios on energy and exergy terms in a direct injection SI hydrogen fueled engine. Int J Hydrogen Energy 2013;38(2):1189–99. https://doi.org/10.1016/j.ijhydene.2012.10.083.
[27] Zanforlin S, Frigo S. Implementation of a novel hydrogen direct-injection concept in single and multi-cylinder engines: CFD, experimental and engine powertrain design studies. Int J Powertrains 2014;3(1):129–50. https://doi.org/10.1504/IJPT.2014.059411.
[28] Maccarley CA. Study of factors influencing thermally induced backfiring in hydrogen fueled engines, and methods for backfire control. Environ Eng Sci 1981;2(16):1449–53. https://www.osti.gov/biblio/5359502.
[29] Ortiz-Imedio R, Ortiz A, Ortiz I. Comprehensive analysis of the combustion of low carbon fuels (hydrogen, methane and coke oven gas) in a spark ignition engine through CFD modelling. Energy Convers Manag 2022;251:114918. https://doi.org/10.1016/j.enconman.2021.114918.
[30] Verhelst S, Wallner T. Hydrogen-Fueled internal combustion engines. Prog Energy Combust Sci 2009;35:490–527. https://doi.org/10.1016/j.pecs.2009.08.001.
[31] Lee S, Kim G, Bae C. Effect of mixture formation mode on the combustion and emission characteristics in a hydrogen direct-injection engine under different load conditions. Appl Therm Eng 2022;209:118276. https://doi.org/10.1016/j.applthermaleng.2022.118276.
[32] Olavson LG, Baker NR, Lynch FE, Mejia LC. Hydrogen fuel for underground mining machinery. SAE Int. J. Engines 1984;93:109–24. https://doi.org/10.4271/840233.
[33] Luo Q, Hu JB, Sun BG, Liu FS, Wang X, Li C, Bao LZ. Experimental investigation of combustion characteristics and NOx emission of a turbocharged hydrogen internal combustion engine. Int J Hydrogen Energy 2019;44:5573–84. https://doi.org/10.1016/j.ijhydene.2018.08.184.
[34] Barış O, Güler İ, Yaşgül A. The effect of different charging concepts on hydrogen fuelled internal combustion engines. Fuel 2023;343:127983. https://doi.org/10.1016/j.fuel.2023.127983.
[35] Wallner T, Matthias NS, Scarcelli R. Influence of injection strategy in a high-efficiency hydrogen direct injection engine. SAE Int. J. Engines 2011;5(1):289–300. https://doi.org/10.4271/2011-01-2001.
[36] Wallner T, Nande AM, Naber JD. Study of basic injection configurations using a direct-injection hydrogen research engine. Proceedings of the 2nd International Conference on Manufacturing Engineering, Quality and Production Systems 2010. https://doi.org/10.4271/2009-01-1418.
[37] Smith GP, Golden DM, Frenklach M, Moriarty NW, Eiteneer B, Goldenberg M, Bowman CT, Hanson RK, Song S, Gardiner WC Jr., Lissianski VV, Qin Z. GRI-MECH Mechanism 3.0. [Internet]. University of Berkeley, California. Available from: http://www.me.berkeley.edu/gri_mech/.
[38] R1 ANSYS Forte theory manual. ANSYS; 2021.
[39] Heywood JB. Internal combustion engine fundamentals. McGraw Hill Series in Mechanical Engineering 1988.
[40] Stan LC, Mitu DE. Simplified mechanism used to estimate the NOx emission of Diesel engine. SAE International 2009;2(1):1221–30. https://doi.org/10.4271/2009-01-1418.
[41] Sahoo S, Srivastava DK. Numerical analysis of performance, combustion, and emission characteristics of PFI gasoline, PFI CNG, and DI CNG engine. Energy 2023;278:127749. https://doi.org/10.1016/j.energy.2023.127749.
[42] Welch A, Mumford D, Munshi S, Holbery J, Boyer B, Younkins M, Jung H. Challenges in developing hydrogen direct injection technology for internal combustion engines. SAE International 2008. https://doi.org/10.4271/2008-01-2379.
[43] Gomes Antunes JM, Mikalsen R, Roskilly AP. An experimental study of a direct injection compression ignition hydrogen engine. Int J Hydrogen Energy 2009;34:6516–22. https://doi.org/10.1016/j.ijhydene.2009.05.142.